SAND2013-4522J

Molecular dynamics simulations of uranyl adsorption and structure on the basal surface of muscovite

Stephanie L. Teich-McGoldrick, Jeffery A. Greathouse*, and Randall T. Cygan

Geochemistry Department, Sandia National Laboratories, Albuquerque, New Mexico 87185-0754 USA

**jagreat@sandia.gov*

Molecular dynamics simulations of uranyl adsorption and structure on the basal surface of muscovite

Anthropogenic activities have led to an increased concentration of uranium on the Earth's surface and potentially in the subsurface with the development of nuclear waste repositories. Uranium is soluble in groundwater, and its mobility is strongly affected by the presence of clay minerals in soils and in subsurface sediments. We use molecular dynamics simulations to probe the adsorption of aqueous uranyl (UO_2^{2+}) ions onto the basal surface of muscovite, a suitable proxy for typically ultrafine-grained clay phases. Model systems include the competitive adsorption between potassium counterions and aqueous ions (0.1 M and 1.0 M UO_2Cl_2 , 0.1 M NaCl). We find that for systems with potassium and uranyl ions present, potassium ions dominate the adsorption phenomenon. Potassium ions adsorb entirely as inner-sphere complexes associated with the ditrigonal cavity of the basal surface. Uranyl ions adsorb in two configurations when it is the only ion species present, and in a single configuration in the presence of potassium. The majority of adsorbed uranyl ions are tilted less than 45° relative to the muscovite surface, and are associated with the Si_4Al_2 rings near aluminum substitution sites.

Keywords: mica, uranium, surface charge, electrolyte

Introduction

Uranium is a naturally occurring element that is found at average levels of two parts per million in the Earth's crust, with higher concentrations in certain minerals associated with granitic rocks [1]. Increased concentrations of uranium, many times greater than background level, are associated with anthropogenic activities, and contamination has primarily accumulated due to mining activities for weapons manufacturing and fuel material for electricity production [2]. Understanding the fate of uranium contamination in the environment is important due to its high toxicity and long-lived radioactive isotopes [3].

Once separated from ore, the transport of uranium through the environment is mediated by the flow of groundwater. In the presence of oxygen, uranium occurs in the +6 oxidation state as the aqueous-soluble uranyl ion, UO_2^{2+} [3]. The presence of clays and other adsorbing minerals strongly influences the mobility of uranyl species and its migration from the contamination source [4-6]. Therefore, understanding interactions between mineral surfaces and uranyl ions is important in developing remediation strategies for contaminated sites and developing risk-assessments for long-term radioactive waste storage.

In the present work, we investigate the adsorption of uranyl ions onto the basal surface of the layered mineral muscovite using molecular dynamics (MD) simulation. Muscovite is a highly-charged phyllosilicate mineral composed of a single octahedral (O) alumina sheet sandwiched between two tetrahedral (T) aluminosilicate sheets to form a TOT layer structure. Permanent negative charge results from isomorphic substitution (aluminum for silicon) in the tetrahedral sheets. Charge-balancing potassium ions are located between TOT layers and electrostatically bind adjacent layers together [7]. Because of its highly-ordered stacking layer structure, muscovite can be easily cleaved along its layers to produce large single crystals that are amenable to microscopic and spectroscopic investigation of its basal surface properties. Additionally, the availability of single crystal X-ray structures [8-12] provides an opportunity to validate MD simulation and other computational methods used to model bulk and interfacial structures of muscovite. Clay minerals, which are ultrafine-grained and typically dominate many sediment environments, have TOT layer structures similar to muscovite but with lower layer charge.

Uranyl adsorption on clay minerals has been studied previously with both experimental and simulation techniques. Greathouse and Cygan have studied uranyl adsorption on external basal surfaces of clay minerals in the presence of carbonate and sodium ions using MD simulations [13, 14]. Experimentally, uranyl adsorption onto

muscovite has been studied using a variety of techniques. Second harmonic generation (SHG) has been used to determine the free energies of adsorption and the surface-active uranyl species bound to muscovite over a range of environmentally-relevant pH values and carbonate concentrations [15-17]. Also, SHG methods can assess the charge density of the muscovite surface and response of the charged solution species. Moyes et al. used X-ray adsorption spectroscopy to show that, at concentrations ranging from 0.025 to 1.0 mM, uranyl ions adsorb to the muscovite surface potentially forming a new phase [11]. Arnold et al. used time-resolved laser-induced fluorescence spectroscopy and high-angle annular dark-field scanning transmission electron microscopy to examine the adsorption of uranyl ions onto muscovite platelets and suspensions [18]. In contrast to Moyes et al., Arnold et al. found that uranyl only adsorbed to the basal surface of muscovite, which was attributed to the lower concentration (1×10^{-5} M) used to obtain the fluorescence spectra. Clearly, there are still questions remaining as to how uranyl ions adsorb to muscovite surfaces.

In this work, we use MD simulation to explore the adsorption of uranyl ions on the muscovite basal surface, specifically the structure of uranyl surface complexes in the presence of electrolyte solutions.

Molecular Model

Our model of the muscovite-solution interface (Figure 1) was created as follows. First, the ideal monoclinic $C2/c$ ($2M_1$ polytype) muscovite structure was constructed from the single crystal X-ray data of Kuwahara [9] and Catti [8]. The experimentally-derived structures do not locate charge substitution sites, therefore, we replaced aluminum for silicon in the tetrahedral sheet to produce a unit-cell formula of $KAl_2(Si_3Al)O_{10}(OH)_2$ with a layer charge of -1.0 e/ unit cell, where e is the electron charge. Lowenstein's rule [19] was obeyed in the

selection of charge sites, and, accordingly, no oxygen atoms bridged two tetrahedrally-substituted aluminum ions. This resulted in a tetrahedral sheet structure having equal proportions of Si_4Al_2 and Si_5Al_1 rings that form ditrigonal cavities on the muscovite surface. Charge-balancing potassium ions were positioned in the interlayer between a Si_4Al_2 ring and a Si_5Al_1 ring.

Following construction of the unit cell, a larger muscovite model was created by expanding the unit cell by 8 x 4 x 2 in the *a*, *b*, and *c* dimensions. The simulation cell was then orthogonalized, resulting in final cell dimensions of 41.6 Å x 36.1 Å x 40.0 Å. An external basal surface was created by cleaving the bulk muscovite structure, and the interlayer potassium counterions were distributed equally across the two exposed basal surfaces. An aqueous region was created by placing 2520 randomized, flexible SPC water molecules [20] above the uppermost basal surface. Counterions in the aqueous region were initially placed above the water layer far from the muscovite surface (Figure 1) to minimize any biasing effects from the initial configuration since the potassium ions bind quite strongly to the muscovite surface even in the presence of water [15]. The bottom muscovite layer was held fixed during the simulation to prevent unwanted collective translation of the system.

Molecular Dynamics Simulation Method

MD simulations of muscovite-aqueous solution interfaces were performed in the canonical (*NVT*) ensemble using the LAMMPS software code [21]. A *slab* geometry was used, leaving the system fully periodic in the *x* and *y* directions but non-periodic in the *z* direction [22] .The slab was terminated by a Lennard-Jones (LJ) 9-3 wall above the water region, and a (virtual) vacuum gap equal to three times the *c* dimension ensures no long-range electrostatic interactions between adjacent slabs. The location of the LJ wall is set such that the water density is equal to 1.0 $g \cdot cm^{-3}$. Long-range electrostatics were treated with the PPPM method

[23] using a precision of 0.0001, and inter-slab dipole interactions were removed. The rRESPA multi-timescale integrator [24] was used to evaluate the intramolecular and short-range intermolecular interactions at 0.5 fs, while the *k*-space interactions were evaluated every 1.0 fs. The Nosé-Hoover thermostat was used with a relaxation time of 100 fs at a temperature T = 298 K. Cutoffs for both LJ and real-space electrostatic interactions were set to 10.0 Å.

Muscovite and monvalent ions (Na^+, K^+, Cl^-) were modeled using Clayff – a flexible force field that describes hydrated mineral systems through primarily non-bonded electrostatic and LJ interactions [25]. Clayff also incorporates the flexible SPC water model of Teleman and Jönsoon[20], which was used to model the water molecules in our system. Uranyl ions (UO_2^{2+}) were modeled using the parameters of Guilbaud and Wipff [26].

Five muscovite-aqueous solution systems were simulated in this study and are distinguished by the composition of the counterion and electrolyte solution, as listed in Table 1. In this context, "counterion" refers to the aqueous ion whose net positive charge balances the net charge of the muscovite supercell (charge density of $-0.346\ C\cdot m^{-2}$). This results in either 32 potassium counterions or 16 uranyl counterions in the aqueous region to maintain charge neutrality. Additional electrolyte was added to create either a 0.1 M (5 ion pairs) or 1.0 M (45 ion pairs) electrolyte concentration. Each simulation was initially energy-minimized before a 10 ns MD simulation was performed. Atomic coordinates were collected every 2 ps over the final 8 ns simulation time.

Results and Discussion

Interfacial structure and trends in ion adsorption can be explored by examining one-dimensional density profiles. Figure 2 includes atomic density profiles and surface charge

profiles generated by time-averaged distributions of ions near the muscovite basal surface. The muscovite surface is defined by the average *z* position of the basal aluminosilicate oxygen atoms. Data are plotted up to 8 Å away from the surface, marking the boundary between the adsorbed and diffuse aqueous regions. Charge density profiles illustrate both the instantaneous charge density and the cumulative charge density (including the surface charge).

The high electric field created by adsorbed divalent uranyl ions (with a +2.5 partial charge on uranium) resulted in localized distortions of the muscovite surface at the tetrahedral aluminum sites, indicating that the force field was unable to maintain the structural integrity of the mineral basal structure in this case. No local structural distortions were observed for systems with the adsorbed singly-charged potassium ions. Therefore, for the MD simulation with uranyl counterions and no other aqueous ions, the entire clay substrate was constrained to remain rigid. For all other simulations, there was no observed distortion of the clay surface and the conventional implementation of Clayff was followed.

The model system denoted "K^+" in Figure 2 represents a cleaved, hydrated muscovite surface and has been studied by X-ray reflectivity experiments [10, 12], classical simulation [27-31], and ab initio molecular dynamics [32]. In particular, comparison with the interfacial structure obtained from X-reflectivity experiments serves to validate our simulation methods. The potassium peak at 1.5 Å indicates a single layer of adsorbed potassium ions forming inner-sphere surface complexes. These potassium ions are centered over ditrigonal cavities on the surface, as discussed below. Our potassium-surface distance is slightly shorter than the value of 1.7 Å obtained from a similar MD simulation using Clayff [31], but the model systems differ in the arrangement of tetrahedral aluminum sites and system size. X-ray reflectivity experiments indicate the same surface structure, with the potassium-surface distance varying from 1.6 Å to 1.9 Å depending on the aqueous potassium concentration [12,

33]. Other classical simulations show varying results depending on the potential parameters used for ion-water and ion-clay interactions. The surface structure reported by Sakuma and Kawamura [30] are consistent with our results, with a potassium-surface distance of 1.7 Å. However, atomic density profiles based on the potassium-water potential of Bounds [34] and either the MCY [35] or TIP4P [36] water model vary considerably. For the MCY-based model, both inner-sphere and outer-sphere potassium surface complexes are seen at 2.1 Å and 2.5 Å, respectively [28]. Results based on the TIP4P water model show inner-sphere potassium adsorption directly over tetrahedral substitution sites at 1.9 Å [27]. Potassium interactions in Clayff are taken from the potassium-water potential of Koneshan et al [37], which was derived from cluster models and successfully reproduces dynamical properties of hydrated potassium ions. Our results showing that potassium adsorbs as an inner-sphere surface complex centered over ditrigonal cavities is consistent with available experimental data and provide a validated underpinning for extending our simulation methods to study uranyl adsorption.

When uranyl ions are the sole aqueous species (denoted "UO_2^{2+}" in Figure 2), two distinct uranyl surface complexes are observed in the simulations. The first uranium peak is located approximately 2.0 Å from the surface while the second broader peak is located at approximately 3.25 Å. The accompanying oxygen peaks indicate a complex adsorption structure, which is investigated in detail below using angular orientations and two-dimensional surface densities.

The remaining density profiles in Figure 2 represent competitive adsorption between potassium counterions and either sodium chloride or uranyl chloride solutions. The potassium peak at 1.7 Å is unaffected by the presence of other aqueous ions, even when these ions are present at a higher concentration (1.0 M). Adsorbed sodium ions form two peaks, each corresponding to inner-sphere surface complexes within the ditrigonal cavities. The first peak

at 0.5 Å indicates sodium ions centered in the cavity similar to adsorbed potassium ions, while sodium ions at 1.8 Å are more closely coordinated to tetrahedral charge sites. The nonzero density between sodium peaks indicates that these ions move between the two adsorption sites, while the near-zero density above z = 2.5 Å indicates infrequent exchange between adsorbed and diffuse sodium ions. In the mixed potassium-uranyl systems, the uranium peak at 2.0 Å is not present, leaving only the peak at 3.25 Å.

The complex structure of adsorbed uranyl ions can be resolved by examining the angle of elevation made by the approximately linear uranyl oxycation relative to the muscovite surface (Figure 3). If the uranyl ion lies flat on the muscovite surface, the elevation angle is defined as 0° while for a uranyl that is normal to the muscovite surface the elevation angle is 90°. The distribution of uranyl orientations are signified by a broad peak at approximately 40° and sharper peaks at approximately 10° and 70°. Uranyl ions oriented at 40° and exhibit a difference of about 1.85 Å between the z coordinates of the uranyl oxygen atoms. This distance corresponds to the observed difference in peak positions between the third and fourth oxygen peaks centered about the second uranium peak (3.25 Å). Similarly, uranyl ions oriented at 10° lie nearly parallel to the muscovite surface and exhibit a difference of 0.65 Å for the z coordinates of their component oxygen atoms. This distance corresponds to the observed distance between the second and third uranyl oxygen peaks centered on the first uranium peak (2.0 Å). Finally, uranyl ions oriented at 70° are nearly perpendicular to the muscovite surface and exhibit a difference of about 3.5 Å in the z coordinates of the oxygen atoms. This distance corresponds to the distance between the first oxygen peak and the beginning of the fourth oxygen peak, which is quite broad, and centered about the second uranium peak (3.25 Å). Examples of these three uranyl-surface orientations are shown in Figure 3.

In both systems with UO_2Cl_2 solutions and potassium counterions, potassium ions are the predominant ions adsorbed directly onto the surface. For the 0.1M UO_2Cl_2 system, only one of the three possible uranyl surface complexes (Figure 3) is observed. The single uranium peak is located at approximately 3.25 Å from the muscovite surface. As the concentration is increased to 1 M UO_2Cl_2, the uranium peak remains at approximately the same distance from the muscovite surface. At both concentrations, uranyl ions are tilted at an angle of 36°, consistent with the associated uranyl orientation shown in Figure 3. Two peaks representing co-adsorbed chloride ions are seen at each UO_2Cl_2 concentration. The second chloride peak shifts closer to the surface along with the uranium peak, indicating ion pairing between uranyl ions and one or two chloride ions.

Areas under the atomic density peaks in Figure 2 were integrated to quantify ion adsorption for each model system (Table 1). The *z* limits for integration were determined from minima in the atomic density profiles. It is evident from these results that potassium is the dominant ion adsorbed onto the muscovite basal surface for all solution compositions. For the systems with no additional electrolyte, nearly all of the counterions are adsorbed. The large electrolyte concentrations used in this study are necessary due to the extremely large system sizes required to model ion concentrations in the millimolar (or less) range often seen in adsorption experiments. As a result, the muscovite surface charge is neutralized within 4 Å for all systems studied. Although X-ray reflectivity experiments indicate that the degree of charge balance depends on electrolyte concentration [12, 33], the effective concentrations modeled here are much larger than those required for partial surface coverage.

The charge density profiles presented in Figure 2 for each of the solution compositions exhibit the instantaneous and cumulative charge as a function of distance from the muscovite surface. Each profile exhibits the initial charge density at the muscovite surface (-0.346 C·m^{-2} at $z = 0$) and the electrical response to the adsorption of various

charged species from the interface to the diffuse region of the aqueous solution near 8 Å, where both instantaneous and cumulative charge approach zero values. Charge density values for the 0.1 M uranyl chloride system are consistent with the experimental conditions from a recent second harmonic generation study of uranyl adsorption on basal surface of muscovite [15]. The occurrence, orientation (for uranyl), and sequence of adsorbate species control the charge density profile. For example, the simple "UO_2^{2+}" system exhibits two steps in the cumulative charge density in response to the two distinct uranyl configurations. Similarly, for simulations with aqueous potassium as the primary counterion, we observe neutralization of the muscovite surface charge by inner sphere potassium adsorption resulting in a sharp increase in the cumulative charge density and a slight positive instantaneous charge density (0.06 C/m^2). This charge density is similar to that reported in SHG experiments of uranyl adsorption on muscovite [15]. Chloride ions involved in ion pairing with the adsorbed potassium (or uranyl) cations occur at distances greater than 3 Å and contribute to balancing any net charge as the diffuse region dominates the interfacial region beyond 8 Å from the basal surface. Table 1 provides cumulative charge densities for each of the aqueous systems evaluated at distances of 8 Å, and which include a correction for the intrinsic surface charge of the muscovite surface.

We also investigated the surface distribution of adsorbed ions to identify adsorption sites relative to tetrahedral charge sites and ditrigonal cavities on the muscovite surface. Potassium ions primarily adsorb in the center of ditrigonal cavities (Figure 4a). Because the MD simulation cell was created by expanding a muscovite unit cell, the charge substitution sites exhibit ordering in the simulation cell with half the ditrigonal rings having two substitution sites (Si_4Al_2) and the other half with one substitution site (Si_5Al_1). As expected, potassium ions predominately bind to cavities with two aluminum substitution sites. This trend is observed for every system containing potassium ions (see Figure 4). For the system

with 1 M NaCl, sodium ions at z = 0.5 Å are also observed in the center of the Si_4Al_2 rings. The more diffuse contour lines of the more distant sodium ions (z = 1.8 Å) indicate a relative mobility in the x and y directions compared to the closer sodium ions, and these ions adsorb between the center of the ditrigonal cavities and the aluminum substitutions sites. As indicated in Table 1, very few uranyl ions adsorbed on the muscovite surface when competing with potassium ions for the same adsorption sites. Those uranyl ions are associated with the Si_4Al_2 rings near both aluminum substitution sites.

Conclusions

We have completed a series of MD simulations to investigate ion adsorption, including uranyl ions, onto the basal surface of muscovite. Potassium ions bind as inner-sphere complexes in a single adsorption peak as illustrated by atomic density profiles, while two distinct adsorption peaks of inner-sphere sodium ions are seen. In the presence of potassium ions, uranyl ions exhibit greatly reduced adsorption than in the absence of potassium ions. Although three possible uranyl-surface orientations are seen in the absence of potassium ions, only the 36° orientation is seen in the presence of potassium ions. Both potassium and uranyl ions adsorb above the Si_4Al_2 rings near aluminum substitution sites. Analysis of adsorbed charge density indicates that inner-sphere potassium adsorption effectively neutralizes the muscovite surface charge, which the presence of other adsorbed cations and anions cause fluctuations in the solution charge density. Ultimately, our MD simulations provide a basis for interpreting spectroscopic data and improving surface adsorption and surface complexation models.

Acknowledgments

We thank Franz Geiger and Sarah (Saslow) Gomez for helpful discussions and comments, and we appreciate the opportunity to examine their recent experimental data for uranyl-muscovite systems. This study was funded by the U.S. Department of Energy, Office of Basic Energy Sciences, Geosciences Research Program. Sandia National Laboratories is a multi-program laboratory operated by Sandia Corporation, a wholly owned subsidiary of Lockheed Martin Corporation, for the U.S. Department of Energy's National Nuclear Security Administration under Contract DE-AC04–94AL85000.

References

[1] E.A. Keller, *Environmental Geology*, Prentice Hall, New Jersey, 2000.

[2] K.D. Crowley, and J.F. Ahearne, *Managing the environmental legacy of US nuclear-weapons production - Although the waste from America's arms buildup will never be "cleaned up," human and environmental risks can be reduced and managed*, Am. Sci. 90 (2002), pp. 514-523.

[3] A. Abdelouas, *Uranium mill tailings: Geochemistry, mineralogy, and environmental impact*, Elements 2 (2006), pp. 335-341.

[4] T. Arnold, T. Zorn, H. Zanker, G. Bernhard, and H. Nitsche, *Sorption behavior of U(VI) on phyllite: experiments and modeling*, J. Contam. Hydrol. 47 (2001), pp. 219-231.

[5] S.Y. Lee, M.H. Baik, and Y.B. Lee, *Adsorption of uranyl ions and microscale distribution on Fe-bearing mica*, App. Clay. Sci. 44 (2009), pp. 259-264.

[6] S.Y. Lee, M.H. Baik, Y.J. Lee, and Y.B. Lee, *Adsorption of U(VI) ions on biotite from aqueous solutions*, App. Clay. Sci. 46 (2009), pp. 255-259.

[7] T. Zoltai, and J.H. Stout, *Mineralogy Concepts and Principles*, Burgess Publishing Company, Minneapolis, 1984.

[8] M. Catti, G. Ferraris, S. Hull, and A. Pavese, *Powder neutron diffraction study of 2M1 muscovite at room pressure and at 2 GPa*, Eur. J. Mineral. 6 (1994), pp. 171-178.

[9] Y. Kuwahara, *Muscovite surface structure imaged by fluid contact mode AFM*, Phys. Chem. Miner. 26 (1999), pp. 198-205.

[10] S.S. Lee, P. Fenter, K.L. Nagy, and N.C. Sturchio, *Monovalent ion adsorption at the muscovite (001)–solution interface: Relationships among ion coverage and speciation, interfacial water structure, and substrate relaxation*, Langmuir 28 (2012), pp. 8637-8650.

[11] L.N. Moyes, R.H. Parkman, J.M. Charnock, D.J. Vaughan, F.R. Livens, C.R. Hughes, and A. Braithwaite, *Uranium uptake from aqueous solution by interaction with goethite, lepidocrocite, muscovite, and mackinawite: An X-ray absorption spectroscopy study*, Environ. Sci. Technol. 34 (2000), pp. 1062-1068.

[12] M.L. Schlegel, K.L. Nagy, P. Fenter, L. Cheng, N.C. Sturchio, and S.D. Jacobsen, *Cation sorption on the muscovite (001) surface in chloride solutions using high-resolution X-ray reflectivity*, Geochim. Cosmochim. Acta 70 (2006), pp. 3549-3565.

[13] J.A. Greathouse, and R.T. Cygan, *Molecular dynamics simulation of uranyl(VI) adsorption equilibria onto an external montmorillonite surface*, Phys. Chem. Chem. Phys. 7 (2005), pp. 3580-3586.

[14] J.A. Greathouse and R.T. Cygan, *Water structure and aqueous uranyl(VI) adsorption equilibria onto external surfaces of beidellite, montmorillonite, and pyrophyllite: Results from molecular simulations*, Environ. Sci. Technol. 40 (2006), pp. 3865-3871.

[15] S.A.S. Gomez, D.S. Jordan, J.M. Troiano, and F.M. Geiger, *Uranyl adsorption at the muscovite (mica/water) interface studied by second harmonic generation*, Environ. Sci. Technol. 46 (2012), pp. 11154-11161.

[16] J.N. Malin, and F.M. Geiger, *Uranyl adsorption and speciation at the fused silica/water interface studied by resonantly enhanced second harmonic generation and the chi((3)) method*, J. Phys. Chem. A 114 (2010), pp. 1797-1805.

[17] J.N. Malin, J.G. Holland, S.A. Saslow, and F.M. Geiger, *Uranyl adsorption and speciation at the acidic silica/water interface studied by resonan and nonresonant second harmonic generation*, J. Phys. Chem. C 115 (2011), pp. 13353-13360.

[18] T. Arnold, S. Utsunomiya, G. Geipel, R.C. Ewing, N. Baumann, and V. Brendler, *Adsorbed U(VI) surface species on muscovite identified by laser fluorescence spectroscopy and transmission electron microscopy*, Environ. Sci. Technol. 40 (2006), pp. 4646-4652.

[19] W. Loewenstein, and M. Lowenstein, *The distribution of aluminum in ihe tetrahedra of silicates and aluminates*, Am. Mineral. 39 (1954).

[20] O. Teleman, B. Jonsson, and S. Engstrom, *A molecular-dynamics simulation of a water model with intramolecular degrees of freedom*, Mol. Phys. 60 (1987), pp. 193-203.

[21] S. Plimpton, *Fast parallel algorithms for short-range molecular-dynamics*, J. Comp. Phys. 117 (1995), pp. 1-19.

[22] I.C. Yeh, and M.L. Berkowitz, *Ewald summation for systems with slab geometry*, J. Chem. Phys. 111 (1999), pp. 3155-3162.

[23] S. Plimpton, R. Pollock, and M. Stevens, *Particle-mesh Ewald and rRESPA for parallel molecular dynamics simulations*, Proceedings Eighth SIAM Conference on Parallel Processing for Scientific Computing (1997).

[24] M.E. Tuckerman, G.J. Martyna, and B.J. Berne, *Molecular-dynamics algorithm for condensed systems with multiple time scales*, J. Chem. Phys. 93 (1990), pp. 1287-1291.

[25] R.T. Cygan, J.J. Liang, and A.G. Kalinichev, *Molecular models of hydroxide, oxyhydroxide, and clay phases and the development of a general force field*, J. Phys. Chem. B 108 (2004), pp. 1255-1266.

[26] P. Guilbaud, and G. Wipff, *Force field representation of the UO22+ cation from free energy MD simulations in water. Tests on its 18-crown-6 and NO3- adducts, and on its calix 6 arene(6-) and CMPO complexes*, J. Mol. Struct. 366 (1996), pp. 55-63.

[27] A. Meleshyn, *Potential of mean force for K^+ in thin water films on cleaved mica*, Langmuir 26 (2010), pp. 13081-13085.

[28] S.H. Park, and G. Sposito, *Structure of water adsorbed on a mica surface*, Phys. Rev. Lett. 89 (2002), pp. 085501.

[29] H. Sakuma, and K. Kawamura, *Structure and dynamics of water on muscovite mica surfaces*, Geochim. Cosmochim. Acta 73 (2009), pp. 4100-4110.

[30] H. Sakuma, and K. Kawamura, *Structure and dynamics of water on Li+-, Na+-, K+-, Cs+-, H3O+-exchanged muscovite surfaces: A molecular dynamics study*, Geochim. Cosmochim. Acta 75 (2011), pp. 63-81.

[31] J.W. Wang, A.G. Kalinichev, R.J. Kirkpatrick, and R.T. Cygan, *Structure, energetics, and dynamics of water adsorbed on the muscovite (001) surface: A molecular dynamics simulation*, J. Phys. Chem. B 109 (2005), pp. 15893.

[32] M. Odelius, M. Bernasconi, and M. Parrinello, *Two dimensional ice adsorbed on mica surface*, Phys. Rev. Lett. 78 (1997), pp. 2855-2858.

[33] S.S. Lee, P. Fenter, K.L. Nagy, and N.C. Sturchio, *Monovalent Ion Adsorption at the Muscovite (001)-Solution Interface: Relationships among Ion Coverage and Speciation, Interfacial Water Structure, and Substrate Relaxation*, Langmuir 28 (2012), pp. 8637-8650.

[34] D.G. Bounds, *A molecular dynamics study of the structure of water around the ions* Li^{+}, Na^{+}, K^{+}, Ca^{++}, Ni^{++}, *and* Cl^{-}, Mol. Phys. 54 (1985), pp. 1335-1355.

[35] O. Matsuoka, E. Clementi, and M. Yoshimine, *CI study of water dimer potential surface*, J. Chem. Phys. 64 (1976), pp. 1351-1361.

[36] W.L. Jorgensen, J. Chandrasekhar, J.D. Madura, R.W. Impey, and M.L. Klein, *Comparison of simple potential functions for simulating liquid water*, J. Chem. Phys. 79 (1983), pp. 926-835.

[37] S. Koneshan, J.C. Rasaiah, R.M. Lynden-Bell, and S.H. Lee, *Solvent structure, dynamics, and ion mobility in aqueous solutions at 25 degrees C*, J. Phys. Chem. B 102 (1998), pp. 4193-4204.

Table 1. Summary of instantaneous charge ($C \cdot m^{-2}$) and percent ion adsorption.

			Instantaneous % adsorbed[b]			
Counterion	Electrolyte	Charge at 8 Å[a]	K^+	UO_2^{2+}	Na^+	Cl^-
K^+	--	−0.02	93	--	--	--
K^+	1 M NaCl	−0.001	75	--	9 (22)	13 (6)
K^+	0.1 M UO_2Cl_2	−0.02	91	16	--	6 (14)
K^+	1.0 M UO_2Cl_2	−0.19	89	5	--	3(4)
UO_2^{2+}	--	−0.01	--	55(40)	--	--

[a]Cumulative charge at 8 Å including the surface charge density.

[b]Percentage of ions contributing to the first peak in the atomic density profiles (Figure 2) with the percentage of ions forming the second peak shown in parenthesis where appropriate.

Figure 1. Snapshots from MD trajectories illustrating the initial configuration (left) and after equilibration (right) for the muscovite-aqueous solution model as viewed along the original *b*-axis of the muscovite. The simulation cell contains 2520 water molecules above the basal surface of a 8 x 4 x 2 muscovite supercell. Aqueous potassium counterions were initially placed above the water layers. Color scheme: oxygen (red), aluminum (pink), silicon (yellow), hydrogen (white), and potassium (purple).

Figure 2. MD-equilibrated atomic density profiles of aqueous species (left) and corresponding charge densities (right) as a function of distance from basal surface of muscovite. Inset graphs show the behavior of species in greater detail. Color scheme for atoms: potassium (purple), uranyl uranium (blue), uranyl oxygen (turquoise), and chlorine (green). For all plots, $z = 0$ corresponds to the average z position of the oxygen atoms of the basal aluminosilicate surface.

Figure 3. Elevation of the uranyl oxycation relative to the muscovite surface with uranyl ions as the sole aqueous species (denoted "UO_2^{2+}" in Figure 2). The schematic illustrates how the elevation angle is measured. The larger peaks at 10° and 70° are associated with uranyl ions adsorbed closest to the muscovite surface, while the shorter peak at 40° is associated with uranyl ions farther from the surface as described in Figure 2. Molecular models show projection and oblique views of a snapshot from the equilibrated MD.

Figure 4. Two-dimensional atomic density distributions of adsorbed cations and tetrahedral silicon and aluminum ions derived from equilibrated MD trajectories. The color scheme is shown in the upper-left-hand corner and is as follows: potassium (purple), aluminum (pink), silicon (yellow), uranium (blue), sodium at $z = 1.8$ Å (black), sodium at $z = 0.5$ Å (dark red). An atomistic snapshot representing a potassium ion adsorbed in the middle of a ditrigonal cavity is provided for reference. Contour lines represent time-averaged atomic distributions averaged in the *xy* plane over the peak width from the one-dimensional atomic profiles.

Figure 1.

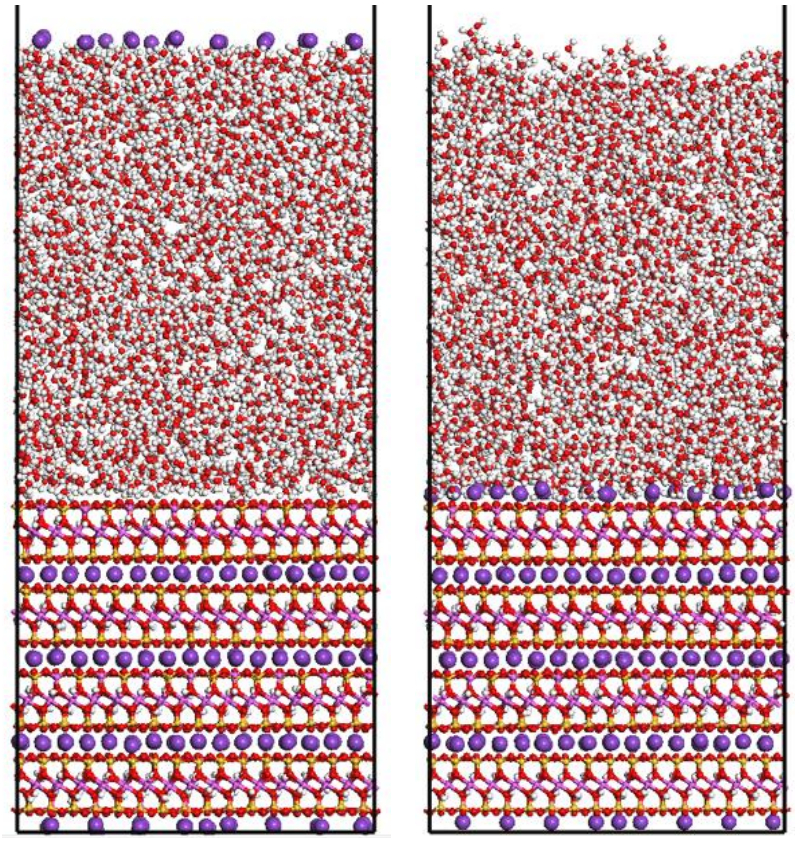

Figure 2

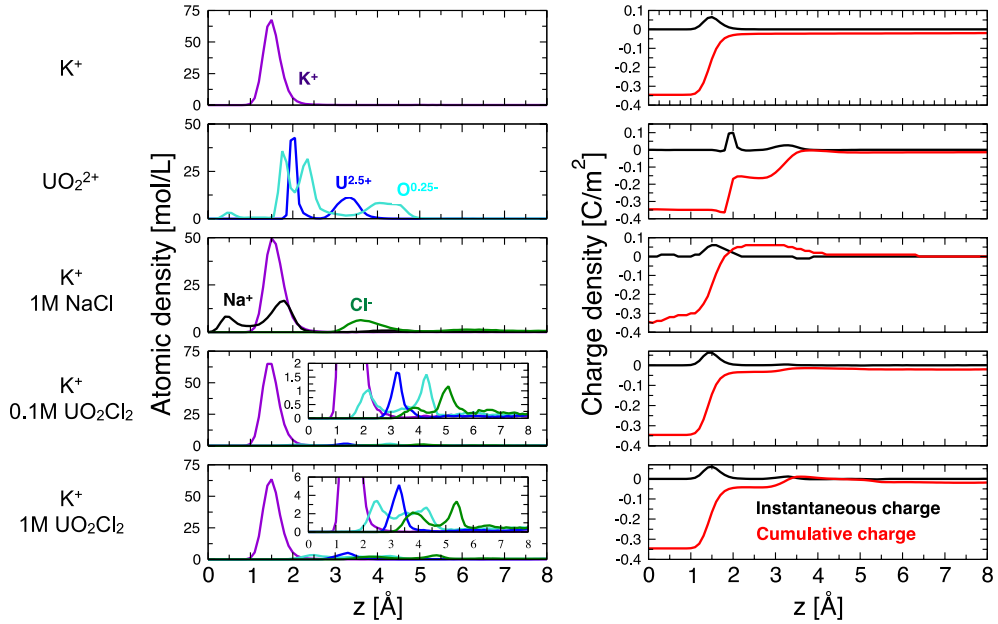
K+
UO2 2+
K+
1M NaCl
K+
0.1M UO2Cl2
K+
1M UO2Cl2
Atomic density [mol/L]
K+
U2.5+
O0.25-
Na+
Cl-
z [Å]
Charge density [C/m2]
Instantaneous charge
Cumulative charge
z [Å]

Figure 3

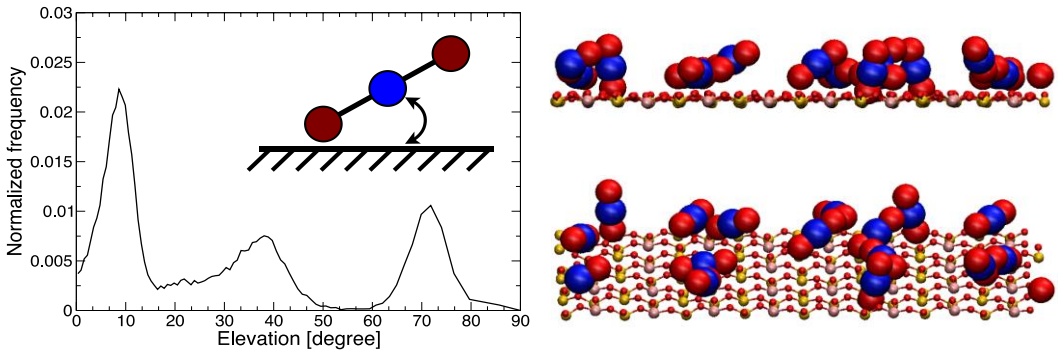
Normalized frequency
0.03
0.025
0.02
0.015
0.01
0.005
0
0
10
20
30
40
50
60
70
80
90
Elevation [degree]

Figure 4

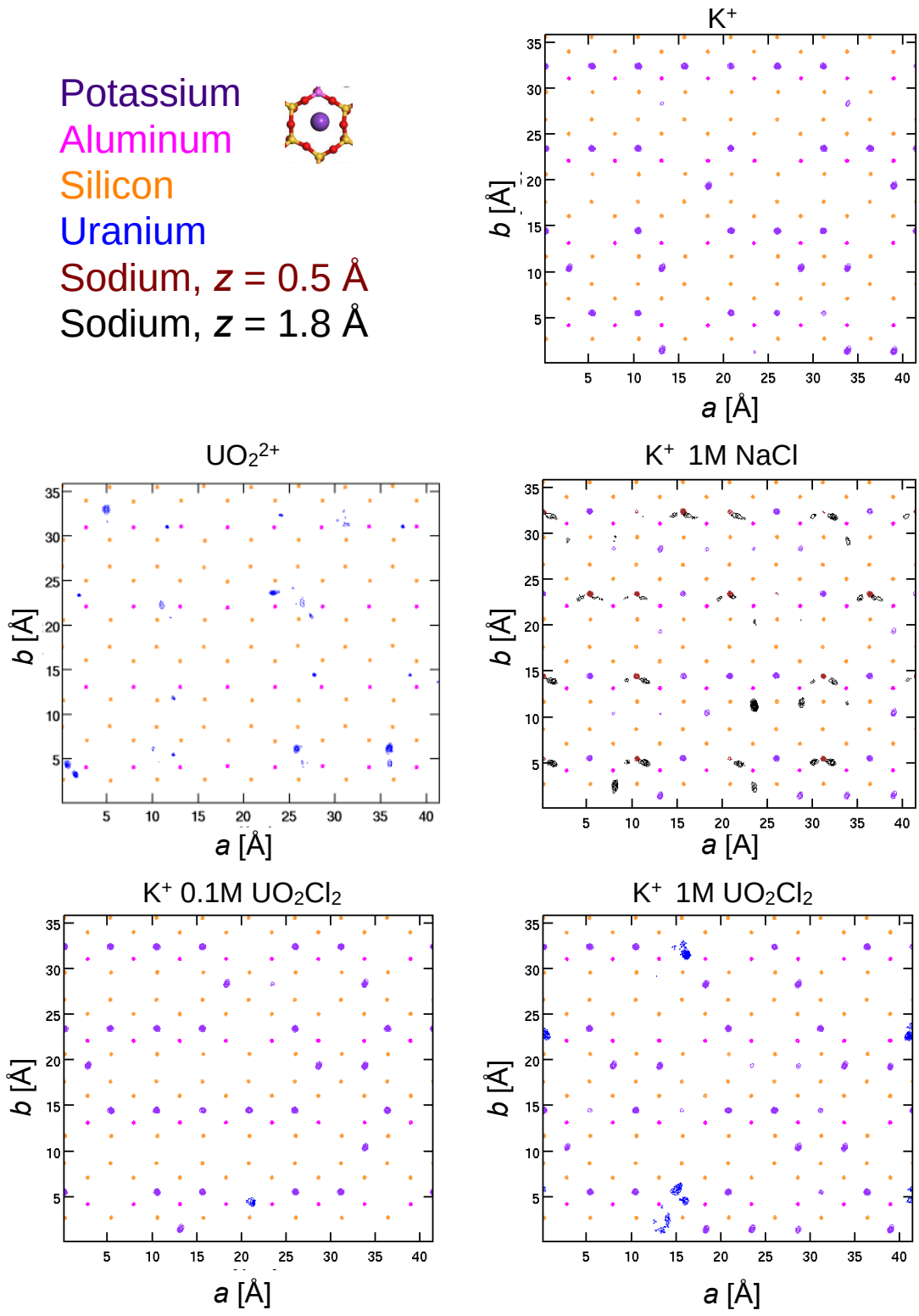
Potassium
Aluminum
Silicon
Uranium
Sodium, z = 0.5 Å
Sodium, z = 1.8 Å
K+
UO2 2+
K+ 1M NaCl
K+ 0.1M UO2Cl2
K+ 1M UO2Cl2
b [Å]
a [Å]